Reprinted from

Canadian Journal of Physics

Réimpression du

Journal canadien de physique

High-resolution laser spectroscopy on the $A^3\Pi \leftarrow X^3\Sigma^-$ transition of NH

W. Ubachs, J. J. ter Meulen, and A. Dymanus

Volume 62 • Number 12 • 1984

Pages 1374–1391

National Research Council Canada
Conseil national de recherches Canada

Printed in Canada by K.G. Campbell Corporation

High-resolution laser spectroscopy on the $A^3\Pi \leftarrow X^3\Sigma^-$ transition of NH

W. UBACHS, J. J. TER MEULEN, AND A. DYMANUS

Fysisch Laboratorium, Katholieke Universiteit Nijmegen, Toernooiveld, 6525 ED Nijmegen, The Netherlands

Received July 7, 1984

In a molecular beam, laser-induced fluorescence experiment, rotational spectra of the $A^3\Pi$, $v = 0 \leftarrow X^3\Sigma^-$, $v = 0$ transition of the NH free radical were measured at 336 nm with high resolution. From more than 300 completely resolved hyperfine lines, the hyperfine structure of the $A^3\Pi$ excited state and the $X^3\Sigma$ ground state could be analyzed. For the first time, the hyperfine coupling constants $a_{N,H}$, $b_{N,H}$, $c_{N,H}$, $d_{N,H}$, eQq_1, and eQq_2 in the $A^3\Pi$ state were determined. Also, the nuclear quadrupole coupling constant eQq_1 in the $X^3\Sigma$ ground state was obtained.

Une expérience de fluorescence induite par un laser à faisceau moléculaire a permis de mesurer, à haute résolution, le spectre rotationnel de la transition $A^3\Pi$, $v = 0 \leftarrow X^3\Sigma$, $v = 0$ du radical libre NH, à 336 nm. A partir de plus de 300 raies hyperfines complètement résolues, on a pu analyser la structure hyperfine de l'état $A^3\Pi$ et de l'état fondamental $X^3\Sigma^-$. Les constantes de couplage hyperfin $a_{N,H}$, $b_{N,H}$, $c_{N,H}$, $d_{N,H}$, eQq_1 et eQq_2 dans l'état $A^3\Pi$ ont été déterminées pour la première fois. On a aussi obtenu la constante de couplage quadrupolaire nucléaire eQq_1 dans l'état fondamental $X^3\Sigma^-$.

[Traduit par le journal]

Can. J. Phys. **62**, 1374 (1984)

1. Introduction

A powerful, highly monochromatic and easily tunable laser system has been developed in our laboratory for the near ultraviolet (uv) (295–340 nm) range (1, 2). In combination with molecular beam techniques, this system allows high-resolution studies of the hyperfine structure of excited electronic states of free radicals. This structure originates from interactions of nuclear multipole moments with internal fields generated by electronic orbital and (or) spin angular momenta and by the electronic charge distribution in the radicals. Typical hyperfine splittings in the excited states are several hundred megahertz. The system has been used recently to study the radicals OH (2) and SH (3). The present communication reports results of the investigation on the hyperfine structure of NH, which is more complex because of its triplet structure and the two contributing nuclear spins.

The NH emission spectrum at 336 nm is well known in astronomy and the earth's atmosphere. Solar observations have been reported by Schadee (4) and observations from many other stars have been reported by Schmitt (5). The appearance of NH in the heads of comets was also established (6). Brewer *et al.* (7) observed enhanced absorption in spectrophotometric measurements on stratospheric ozone at 336 nm and concluded that there is an absorbing layer, probably composed of NH, in the 40–50 km region of the stratosphere.

Spectroscopic studies of the NH radical have a long tradition. More than ninety years ago, Eder (8) investigated the band system at 336 nm. In the thirties, when higher resolution spectrometers were available to resolve the rotational structure, Funke (9) was first to assign the main branches of the strong (0, 0) and (1, 1) bands of the $A^3\Pi - X^3\Sigma$ transition. In 1959 Dixon (10) reported new definitive measurements on the $A^3\Pi - X^3\Sigma^-$ system, including a determination of satellite branches due to the triplet structure and a correction for mistaken identification in Funke's measurements. In the same paper, Dixon gave a complete fine structure analysis of the ground and excited state and obtained accurate rotational constants for both states. The Λ-doubling and spin–spin interaction in $A^3\Pi$ could be described well with the theory given by Hebb (11). The weaker (0, 1), (1, 0), (1, 2), and (2, 1) bands of the $A^3\Pi - X^3\Sigma^-$ system were measured by Malicet *et al.* (12).

Four more singlet states are known for NH, the $a^1\Delta$, $b^1\Sigma^+$, $c^1\Pi$, and $d^1\Sigma^-$ states. Emission spectra from the $c^1\Pi - a^1\Delta$ transition were obtained by Dieke and Blue (13) for the (0, 0) band at 324 nm, and many years later emission spectra for the (0, 1) band were obtained by Ramsay and Sarre (14). Another system, identified as $c^1\Pi - b^1\Sigma^+$, at 450 nm was described by Lunt *et al.* (15). Graham and Lew (16) gave a full analysis of the fine structure of several vibrational bands of the $d^1\Sigma^+ - c^1\Pi$ and $d^1\Sigma^+ - b^1\Sigma^+$ systems. Gilles *et al.* (17) observed the $b^1\Sigma^+ - X^3\Sigma^-$ singlet–triplet transition, which makes it possible to give a complete energy level scheme for all singlet and triplet states.

The advancement of laser techniques opened a new era in high-resolution studies of NH. Bernath and Amano (18) investigated the $v = 0 \rightarrow v = 1$ rotation–vibration spectrum at 3.2 μm in the electronic ground state by using laser radiation produced by frequency mixing of two visible lasers. The hyperfine structure in the $X^3\Sigma$, $v = 0$ and $v = 1$ levels was

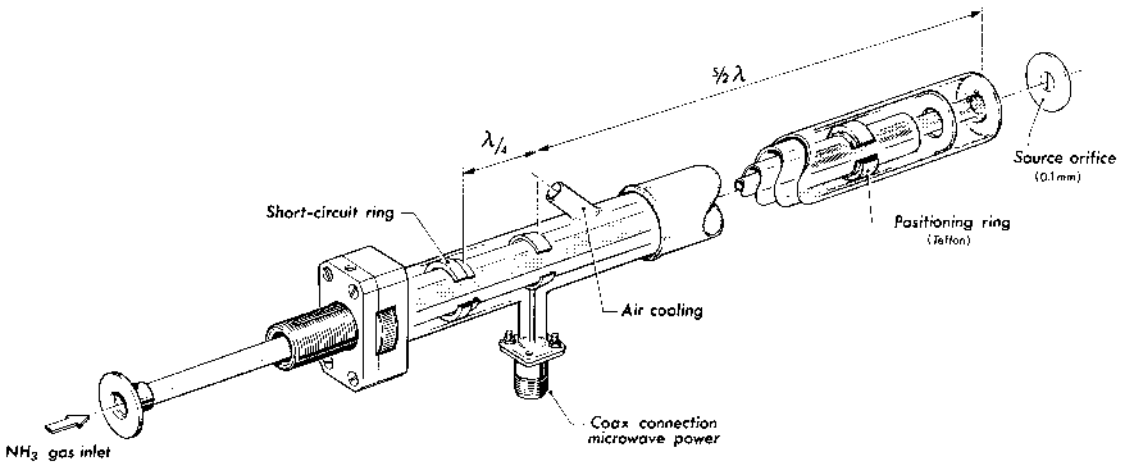

FIG. 1. View of the NH source.

measured by Wayne and Radford (19) in a laser magnetic resonance experiment. Improved hyperfine parameters for the $v = 0$ level were obtained by Van den Heuvel *et al.* (20) from an absorption measurement of tunable far infrared radiation, produced by mixing the output of an HCN laser with microwave radiation on a diode. No laser spectroscopy on the excited $A^3\Pi$ state has been reported yet.

In the present investigation, the hyperfine structure in the electronically excited $A^3\Pi$, $v = 0$ state has been measured for the first time in a laser induced fluorescence (LIF) molecular beam experiment. To our knowledge, it is the first complete determination of the hyperfine structure in a heteronuclear diatomic molecule with two nuclear magnetic moments in a $^3\Pi$ state. Hyperfine splitting of the electronically excited $^3\Pi_1$, $v = 0$, $J = 1$ state of InH was observed in a classical spectroscopic investigation by Neuhaus (21), but the hyperfine structure could not be analyzed in detail because of the low resolution and the complexity of the spectrum. Chow Chiu (22) determined the hyperfine structure of the hydrogen molecule in the metastable $c^3\Pi$ state and Gammon *et al.* (23) did the same for the metastable $a^3\Pi$ state of ^{13}CO.

We induced transitions between rotational levels of the $X^3\Sigma^-$, $v = 0$ ground state and the three $^3\Pi_{0,1,2}$, $v = 0$ excited electronic states; more than 300 hyperfine splittings have been observed. To analyze the data and deduce the hyperfine constants, we extended the theory of the hyperfine structure in a $^3\Pi$ state, as given by Freed (24), to the case of two nuclear spins. As for NH, $A/B = -2.146$, the coupling of the angular momenta is really intermediate between Hund's cases (a) and (b) (25). The hyperfine matrix elements were calculated with symmetrized Hund's case (a) basis functions, and they depend strongly on the mixing coefficients for the $^3\Pi$ wave functions, which have to be determined by diagonalizing the spin-rotation matrix for each J. To obtain a complete description and a good fit of all data to the theoretical expressions, the spin–spin interaction and A-doubling parameters as given by Dixon (10) were included in the spin-rotation matrix of the $A^3\Pi$ state. For the $X^3\Sigma^-$ ground state, the hyperfine matrix elements were calculated with Hund's case (b) wave functions. From a least squares fit, we obtained the hyperfine constants for the NH radical: in the notation of Frosch and Foley (26), $a_{N,H}$, $b_{N,H}$, $c_{N,H}$, and $d_{N,H}$ for both nuclei and eQq_1 and eQq_2 for the nitrogen nucleus in the $A^3\Pi$ state; for the $X^3\Sigma^-$ state we obtained values of $b_{N,H}$, $c_{N,H}$, and eQq_1. The hyperfine constants give direct information about the electronic distribution in the NH molecule. Although much theoretical work has been published about the electronic structure of NH (27), no *ab initio* calculations of the hyperfine constants have been reported except for a calculation of the Fermi-contact term (28). Thus, only a qualitative discussion of the obtained values will be given.

2. Experiment

The NH radicals are produced in a microwave gas discharge in ammonia. The design of the microwave cavity (Fig. 1) is in principle the same as described by Brink *et al.* (29). The dimensions of the two copper cylindrical conductors forming the coaxial cavity are such that a standing wave with a minimum at the short-circuit ring and maxima at the input connector and the far end of the discharge cavity is possible. As the wavelength is 12.5 cm, the length of the cavity was chosen to equal 32.5 cm to fulfill these conditions. The discharge is sustained by about 100 W of broadband microwave power at 2.45 GHz from a microwave generator. A continuous flow of pure NH_3 gas is maintained through the air-cooled pyrex glass tube with an inner diameter of 7 mm. The pink–red flame of the

ammonia discharge can be seen pointing 2 cm out of the cavity. Optimum pressure for NH production is about 6 Torr (1 Torr = 133 Pa) at the inlet and 0.05 Torr above the 500 m^3/h Rootspump. The NH source is mounted close to the beam orifice, which is a 0.1-mm-wide and 2-mm-high boron nitride slit. The discharge flame points through the slit opening so that NH molecules can also be formed in the molecular beam.

The LIF focusing centre, where the excitation of the NH molecules takes place, is at a distance of 15 cm from the source. An adjustable slit diaphragm was installed 6.5 cm behind the beam source. By narrowing this slit to 0.25 mm, a residual Doppler width of 13 MHz could be obtained for the spectral lines, sufficiently small to resolve the hyperfine components of most transitions. The broadening effect of the natural lifetime of the $A^3\Pi$ state (0.3 MHz), as measured by Smith *et al.* (30), is negligible. The molecular beam was chopped at 120 Hz for phase-sensitive detection of the LIF signal.

The UV radiation at $\lambda = 336$ nm was produced by doubling the laser frequency in a $LiIO_3$ crystal in a second focus inside a single-frequency ring dye laser system (1, 2). The original laser system developed for the 295–330 nm tuning range has been modified to overcome the problem of polarization rotation by the $LiIO_3$ crystal at longer wavelengths, because both the wavelength tuning by the Lyot filter and the unidirectional operation depend on the polarization of the light beam inside the cavity. In the modified design, the quartz plate, which together with the Faraday rotator normally forms the unidirectional device of the ring laser, has been removed; its function was taken over by the optically active $LiIO_3$ crystal. The optical activity in $LiIO_3$ is found to depend on the tuning of a second angle ϕ, which is not used in the angle tuning to reach phase-matching conditions for the UV production. This property originates in the hexagonal symmetry of $LiIO_3$, which makes it possible to reach phase-matching conditions by rotating only one angle (1).

The UV output power was 0.5 mW at 5-W pump power in all lines from an Ar–ion laser. The laser line width was 0.5 MHz, root-mean-square (rms). The spectra were recorded relative to the markers of a pressure and temperature stabilized interferometer with a free spectral range of 299.41 ± 0.02 MHz.

3. Theory

The Hamiltonian for the NH molecule in the $^3\Pi$ electronic state may be written formally as

$$[1] \qquad \mathbf{H} = \mathbf{H}_0 + \mathbf{H}_f + \mathbf{H}_{hf}$$

The nonrelativistic Hamiltonian $\mathbf{H}_0$ gives the electronic and vibrational energies; $\mathbf{H}_f$ is the fine structure Hamiltonian describing the rotational structure, triplet splitting, and Λ-doubling; and $\mathbf{H}_{hf}$ is the hyperfine Hamiltonian containing the interactions with the nuclear spins and the quadrupole moment of the nitrogen nucleus. For $\mathbf{H}_f$ the expression used is

$$[2] \qquad \mathbf{H}_f = A\boldsymbol{L}\cdot\boldsymbol{S} + B(\boldsymbol{J} - \boldsymbol{L} - \boldsymbol{S})^2 + \mathbf{H}_{ss}$$

Here $\boldsymbol{L}$ and $\boldsymbol{S}$ are the electronic-orbital angular momentum and spin respectively; $\boldsymbol{J}$ is the total rotational angular momentum of the molecule, excluding the nuclear spins, and $\mathbf{H}_{ss}$ represents the electronic spin–spin interaction. The hyperfine Hamiltonian, expressed in the single-electron operators $T^{(1)}(s_i)$ and their orbital analogues $T^{(1)}(l_i)$, has the following form (24):

$$[3] \qquad \mathbf{H}_{hf} = \sum_{i,k,q} \zeta_k (-1)^q T_q^{(1)}(I_k) T_{-q}^{(1)}(l_i)/r_{ik}^3 + \sqrt{30} \sum_{i,k,q,\mu} \zeta_k \begin{pmatrix} 1 & 1 & 2 \\ \mu & q-\mu & -q \end{pmatrix} T_\mu^{(1)}(s_i) T_{q-\mu}^{(1)}(I_k)$$
$$\times C_{-q}^{(2)}(\theta_{ik}, \phi_{ik})/r_{ik}^3 + \frac{8\pi}{3} \sum_{i,k,q} \zeta_k (-1)^q T_q^{(1)}(I_k) T_{-q}^{(1)}(s_i) \delta(r_{ik}) + \sum_{i,q} (-1)^q T_q^{(2)}(Q) T_{-q}^{(2)}(V_i)$$

with $\zeta_k = g\, g_k \mu_B \mu_N$ where g, g_k, μ_B, and μ_N are the g values for the free electron, the nucleus k, the Bohr magneton, and the nuclear magneton respectively. The indices i and k refer to electrons and nuclei respectively; r_{ik} is the distance between electron i and nucleus k; θ_{ik} is the angle between r_{ik} and the internuclear axis; and ϕ_{ik} is the azimuthal angle. The first three terms of $\mathbf{H}_{hf}$ represent the interaction between the nuclear magnetic moments and the magnetic field produced by the electronic orbital and spin angular momentum at the place of the nuclei; the third contribution is the Fermi-contact term. The last term is the interaction between the quadrupole moment Q of the nitrogen nucleus and the electric field gradient due to the hydrogen nucleus and the electrons. Not included in $\mathbf{H}_{hf}$ are the nuclear spin-rotation and nuclear spin–spin interactions, which give contributions far below the experimental accuracy.

The hyperfine Hamiltonian can be considered as a small perturbation on $\mathbf{H}_f$, and consequently the hyperfine energies can be calculated using the eigenfunctions

TABLE 1. Matrix elements of $\mathbf{H}_f$ between the symmetrized $^3\Pi^{\pm}_{\Omega}$ states. The constants α, κ, ξ, and η are defined in the text; $x = J(J+1)$

	$^3\Pi_2^{\pm}$	$^3\Pi_1^{\pm}$	$^3\Pi_0^{\mp}$
$^3\Pi_2^{\pm}$	$A + B(x-3) + \lvert\eta\rvert^2(x-2)$	$-B\sqrt{2(x-2)} - \xi^*\eta\sqrt{(x-2)/2}$	$\pm\lvert\eta\rvert^2\sqrt{x(x-2)}$
$^3\Pi_1^{\mp}$	$-B\sqrt{2(x-2)} - \xi\eta^*\sqrt{(x-2)/2}$	$B(x+1) + \frac{1}{2}\lvert\xi\rvert^2 + (1 \pm 1)^2\frac{1}{2}\lvert\eta\rvert^2 x$	$-B\sqrt{2x} \mp \xi\eta^*\sqrt{\frac{1}{2}x} - (1 \pm 1)^2\xi^*\eta\sqrt{x/8}$
$^3\Pi_0^{\pm}$	$\pm\lvert\eta\rvert^2\sqrt{x(x-2)}$	$-B\sqrt{2x} \mp \xi^*\eta\sqrt{\frac{1}{2}x} - (1 \pm 1)^2\xi\eta^*\sqrt{x/8}$	$-A + B(x+1) \mp \alpha - (1 \pm 1)\kappa + \lvert\eta\rvert^2 x + (1 \pm 1)^2\frac{1}{2}\lvert\xi\rvert^2$

of $\mathbf{H}_f$. These are obtained by diagonalizing the $\mathbf{H}_f$ matrix based on symmetrized Hund's case (a) functions,

$$[4] \qquad |^3\Pi^{\pm}_{|\Omega|} J M_J\rangle = \frac{1}{\sqrt{2}}(|\Lambda\Sigma\Omega J M_J\rangle \pm |-\Lambda - \Sigma - \Omega J M_J\rangle)$$

with Λ and Σ the projections of $\boldsymbol{L}$ and $\boldsymbol{S}$ on the internuclear axis, and $\Omega = \Lambda + \Sigma$. The case ($a$) wavefunctions can be split into an electronic and a rotational part,

$$[5] \qquad |\Lambda\Sigma\Omega J M_J\rangle = |\Lambda\Sigma\rangle|J\Omega M_J\rangle$$

with

$$|J\Omega M_J\rangle = (-1)^{M_J-\Omega}\sqrt{\frac{2J+1}{8\pi^2}}D^{(J)}_{M_J\Omega}(\alpha,\beta,\gamma)$$

The symmetry of the wave functions [4] under a reflection σ_{xz} in a plane containing the internuclear axis is

$$[6] \qquad \sigma_{xz}|^3\Pi^{\pm}_{|\Omega|} J M_J\rangle = \pm(-1)^J|^3\Pi^{\pm}_{|\Omega|} J M_J\rangle$$

as discussed in Appendix A.

Using the phase convention for $\mathbf{S}$, $\mathbf{L}$, and $\mathbf{J}$ given by Edmonds (31), the matrix elements of $\mathbf{H}_f$ are obtained as given in Table 1. Included in the matrix are the interactions with the $X^3\Sigma^-$ and $b^1\Sigma^+$ states, which, according to Dixon (10), give the dominating contributions to the Λ-doubling in the $^3\Pi$ state. The matrix elements of the interaction with $X^3\Sigma^-$ are calculated in the way pointed out by Freed (24). The constants ξ and η are

$$[7] \qquad \xi = \langle\Lambda = 1|(A + 2B)\tilde{\mathbf{L}}_+|\Lambda = 0\rangle/\sqrt{E(\Pi,\Sigma)}$$
$$\eta = \langle\Lambda = 1|B\tilde{\mathbf{L}}_+|\Lambda = 0\rangle/\sqrt{E(\Pi,\Sigma)}$$

with $E(\Pi,\Sigma)$ the separation between the $A^3\Pi$ and $X^3\Sigma$ states. In the pure precession approximation, which Dixon found to be approximately true, he obtained the values $\xi\eta = 0.0012\ \text{cm}^{-1}$ and $|\eta|^2 = 0.0159\ \text{cm}^{-1}$, while $|\xi|^2$ is very small because accidentally A is nearly equal to $-2B$. The $b^1\Sigma^+$ state interacts only with $^3\Pi_0^+$ via the spin-orbit coupling and gives a constant negative shift κ independent of J. Also, the spin–spin interaction gives a J independent splitting, $\pm\alpha$, of the $^3\Pi_0$ state (11). It turns out that $|\kappa + 2\alpha|$ is almost equal to the Λ-doublet splitting in the $^3\Pi_0$, $J = 0$ state for which Dixon obtained a value of 2.63 cm^{-1}.

For κ we used the value of $-1.6\ \text{cm}^{-1}$ derived by Dixon with a rather large error of 0.3 cm^{-1}, which is, however, acceptable in view of the small influence of κ on the eigenfunctions of $\mathbf{H}_f$. Freed has also considered the interactions with other excited electronic states such as $^1\Delta$ and $^1\Pi$, which may also give a contribution to the Λ-doubling of the $^3\Pi$ states. However, no experimental data for these interactions are available. Some of the matrix elements given by Freed differ in sign with our expressions; this is due to phase differences in the symmetrized basis functions and the matrix elements of $\mathbf{S}_+$. Diagonalization of $\mathbf{H}_f$ gives the eigenfunctions that are linear combinations of the symmetrized basis functions:

$$[8] \qquad |^3\Pi^{\pm}_{i\Omega|}, J\rangle = \sum_{\Omega'=0,1,2} S_{\Omega,\Omega'}(J)|^3\Pi^{+}_{|\Omega'|}, J\rangle$$

With $A = -35.02\ \text{cm}^{-1}$ and $B = 16.322\ \text{cm}^{-1}$ (10), the resulting values for the S coefficients are all of the same order of magnitude so we deal with a typical intermediate coupling case.

The matrix elements of the hyperfine Hamiltonian [3] are calculated in the reduced electron density approximations of McWeeny (32) by applying the normalized spin and orbital density functions $D_S(\Sigma,\Sigma'|r)$ and $D_L(\Lambda,\Lambda'|r)$. The basis wave functions are products of the functions $|^3\Pi^{\pm}_{i\Omega|}, J\rangle$ and the nuclear spin functions $|I_1F_1I_2FM_F\rangle$ using the coupling scheme $J + I_1 = F_1$, $F_1 + I_2 = F$ with $I_1 = 1$, the spin of the nitrogen nucleus, $I_2 = 1/2$, the proton spin, and F, the total molecular angular momentum. The resulting expressions are diagonal in F.

$$\langle {}^3\Pi^{\pm}_{|\Omega|} J I_1 F_1 I_2 F | \mathbf{H}_{hf} | {}^3\Pi^{+}_{|\Omega|} J I_1 F_1' = F_1 I_2 F \rangle = g_1(J, I_1, F_1)\Big[a_1 X_a(\Omega, J) + b_{F_1} X_b(\Omega, J) + \frac{1}{3} c_1 X_c(\Omega, J) \pm d_1 X_d(\Omega, J) \Big] + g_2(J, I_1, F_1, I_2, F)\Big[a_2 X_a(\Omega, J) + b_{F_2} X_b(\Omega, J) + \frac{1}{3} c_2 X_c(\Omega, J) \pm d_2 X_d(\Omega, J) \Big] + g_3(J, I_1, F_1)[eQq_1 X_e(\Omega, J) \pm eQq_2 X_f(\Omega, J)] \quad [9]$$

$$\langle {}^3\Pi^{\pm}_{|\Omega|} J I_1 F_1 I_2 F | \mathbf{H}_{hf} | {}^3\Pi^{+}_{|\Omega|} J I_1 F_1' = (F_1 + 1) I_2 F \rangle = g_4(J, I_1, F_1, I_2, F)\Big[a_2 X_a(\Omega, J) + b_{F_2} X_b(\Omega, J) + \frac{1}{3} c_2 X_c(\Omega, J) \pm d_2 X_d(\Omega, J) \Big]$$

Here

$$g_1(J, I_1, F_1) = \frac{F_1(F_1 + 1) - J(J + 1) - I_1(I_1 + 1)}{2J(J + 1)}$$

$$g_2(J, I_1, F_1, I_2, F) = \frac{[F_1(F_1 + 1) + J(J + 1) - I_1(I_1 + 1)]}{2J(J + 1)} \cdot \frac{[F(F + 1) - F_1(F_1 + 1) - I_2(I_2 + 1)]}{2F_1(F_1 + 1)}$$

$$g_3(J, I_1, F_1) = \frac{3Y(Y - 1) - 4J(J + 1)I_1(I_1 + 1)}{(2J - 1)(2J)(2J + 2)(2J + 3)(2I_1)(2I_1 - 1)}$$

$$g_4(J, I_1, F_1, I_2, F) = -\Big[\frac{(J + I_1 + F_1 + 2)(J - I_1 + F_1 + 1)}{(2F_1 + 1)(2F_1 + 3)} \times (-J + I_1 + F_1 + 1)(J + I_1 - F_1)(F_1 + I_2 + F + 2)(F_1 + I_2 - F + 1) \times (F_1 - I_2 + F + 1)(F - F_1 + I_2) \Big]^{1/2} \frac{1}{4J(J + 1)(F_1 + 1)}$$

$$X_a(\Omega, J) = S_{\Omega,1}(J)^2 + 2S_{\Omega,2}(J)^2$$

$$X_b(\Omega, J) = 2S_{\Omega,2}(J)^2 + \sqrt{2X - 4}\, S_{\Omega,1}(J) S_{\Omega,2}(J) + \sqrt{2X}\, S_{\Omega,1}(J) S_{\Omega,0}(J)$$

$$X_c(\Omega, J) = 4S_{\Omega,2}(J)^2 - \sqrt{2X - 4}\, S_{\Omega,1}(J) S_{\Omega,2}(J) - \sqrt{2X}\, S_{\Omega,1}(J) S_{\Omega,0}(J)$$

$$X_d(\Omega, J) = \sqrt{2X}\, S_{\Omega,0}(J) S_{\Omega,1}(J)$$

$$X_e(\Omega, J) = 3S_{\Omega,1}(J)^2 + 12S_{\Omega,2}(J)^2 - X$$

$$X_f(\Omega, J) = \frac{X}{2} S_{\Omega,1}(J)^2 + 2\sqrt{X(X - 2)}\, S_{\Omega,2}(J) S_{\Omega,0}(J)$$

with $X = J(J + 1)$ and $Y = I_1(I_1 + 1) + J(J + 1) - F_1(F_1 + 1)$. a_k, b_{F_k}, c_k, and d_k are the magnetic hyperfine coupling constants of Frosch and Foley (26), and q_1 and q_2 are the quadrupole coupling constants related to the expectation values of electronic operators (33).

$$a_k = \zeta_k \int \frac{1}{r_{1k}^3} D_K(\Lambda, \Lambda/r_{1k})\, d\mathbf{r}_{1k}$$

$$b_{F_k} = \frac{8}{3} \pi \zeta_k D_S(\Sigma, \Sigma/0)$$

$$c_k = \frac{3}{2} \zeta_k \int \frac{3 \cos^2 \theta_{1k} - 1}{r_{1k}^3} D_S(\Sigma, \Sigma/r_{1k})\, d\mathbf{r}_{1k}$$

$$d_k = \frac{3}{2} \zeta_k \int \frac{\sin^2 \theta_{1k}}{r_{1k}^3} D_S(\Sigma, \Sigma - 1)/r_{1k})\, d\mathbf{r}_{1k} \quad [10]$$

$$q_1 = \frac{2}{R} - \int \frac{3 \cos^2 \theta_{1N} - 1}{r_{1N}^3} D_L(\Lambda, \Lambda/r_{1N})\, d\mathbf{r}_{1N}$$

$$q_2 = -3 \int \frac{\sin^2 \theta_{1N}}{r_{1N}^3} D_L(\Lambda, -\Lambda/r_{1N})\, d\mathbf{r}_{1N}$$

with R the internuclear distance. Matrix elements with $\Delta J \neq 0$ and (or) $\Delta\Omega \neq 0$ are not taken into account since they are expected to give contributions estimated to be smaller than 1 MHz to the hyperfine energies.

For each $^3\Pi_\Omega^\pm$, J state, the hyperfine matrix factors into two 1×1 matrices for $F = J \pm 3/2$ and two 2×2 matrices, one for $F = J + 1/2$ and one for $F = J - 1/2$. Diagonalization gives the hyperfine splittings and the eigenfunctions that are needed for the identification of the spectral components by their relative intensities.

The hyperfine splittings and eigenfunctions of the $X^3\Sigma^-$ ground electronic state of NH are calculated in Hund's case (b) representation using the coupling scheme $\boldsymbol{N} + \boldsymbol{S} = \boldsymbol{J}$, $\boldsymbol{J} + \boldsymbol{I}_1 = \boldsymbol{F}_1$, $\boldsymbol{F}_1 + \boldsymbol{I}_2 = \boldsymbol{F}$. Here $\boldsymbol{N}$ is the angular momentum of the nuclear end-over-end rotation. The hyperfine Hamiltonian contains the same terms as given in [3] except for the $I \cdot L$ interaction, while in the second term a nonzero contribution is obtained only for $q = 0$. The following expressions for the matrix elements of $\mathbf{H}_{hf}$ are obtained:

$$\langle {}^3\Sigma^- N J I_1 F_1 I_2 F | \mathbf{H}_{hf} | {}^3\Sigma^- N J I_1 F_1' = F_1 I_2 F \rangle$$

$$= g_1(J, I_1, F_1)\left[b_{F_1} + \frac{2}{3}c_1\right] + g_2(J, I_1, F_1, I_2, F)\left[b_{F_2} + \frac{2}{3}c_2\right] + g_5(N, J, I_1, F_1)eQq_1 \qquad \text{for } J = N$$

$$= g_1(J, I_1, F_1)\left[-b_{F_1}J + \frac{2}{3}c_1\frac{J(J+2)}{2J+1}\right] + g_2(J, I_1, F_1, I_2, F)\left[-b_{F_2}J + \frac{2}{3}c_2\frac{J(J+2)}{2J+1}\right]$$

$$+ g_5(N, J, I_1, F_1)eQq_1 \qquad \text{for } J = N - 1$$

[11]

$$= g_1(J, I_1, F_1)\left[b_{F_1}(J+1) - \frac{2}{3}c_1\frac{(J+1)(J-1)}{2J+1}\right] + g_2(J, I_1, F_1, I_2, F)$$

$$\times \left[b_{F_2}(J+1) - \frac{2}{3}c_2\frac{(J+1)(J-1)}{2J+1}\right] + g_5(N, J, I_1, F_1)eQq_1 \qquad \text{for } J = N + 1$$

$$\langle {}^3\Sigma^- N J I_1 F_1 I_2 F | \mathbf{H}_{hf} | {}^3\Sigma^- N J I_1 F_1' = (F_1 + 1) I_2 F \rangle = g_4(J, I_1, F_1, I_2, F)\left[b_{F_2} + \frac{2}{3}c_2\right] \qquad \text{for } J = N$$

$$= g_4(J, I_1, F_1, I_2, F)\left[-b_{F_2}J + \frac{2}{3}c_2\frac{J(J+2)}{2J+1}\right] \qquad \text{for } J = N - 1$$

$$= g_4(J, I_1, F_1, I_2, F)\left[b_{F_2}(J+1) - \frac{2}{3}c_2\frac{(J+1)(J-1)}{2J+1}\right] \qquad \text{for } J = N + 1$$

with

$$g_5(N, J, I_1, F_1) = -\frac{[3Z(Z-1) - 4J(J+1)N(N+1)]}{2(2N-1)(2N+3)2I_1(2I_1-1)} \cdot \frac{[3Y(Y-1) - 4J(J+1)I_1(I_1+1)]}{(2J-1)(2J)(2J+2)(2J+3)}$$

where $Z = J(J+1) + N(N+1) - 2$. The magnetic hyperfine coupling constants b_{F_k} and c_k, and the quadrupole coupling constant q_1 have expressions analogous to the ones given in [10] for the $^3\Pi$ state. Following Van den Henvel *et al.* (20), only matrix elements of the type $\Delta J = 0$, $\Delta N = 0$ are considered.

4. Measurements and interpretation

The rotational transitions investigated are $Q_1(N)$ for $N = 1$ to 3, $R_1(N)$ for $N = 0$ and 2 to 7, $^QR_{12}(3)$, $Q_2(1)$, $R_2(3)$, $^QR_{23}(N)$ for $N = 1, 2$, $^RQ_{21}(N)$ for $N = 4$ to 6, $^QP_{21}(N)$ for $N = 1, 2$, $Q_3(N)$ for $N = 4$ to 7, $R_3(N)$ for $N = 1$ to 7, $^QP_{32}(N)$ for $N = 3$ to 6, and $P_3(3)$; N refers to the quantum number of the nuclear rotation in the ground state. The $A^3\Pi_\Omega$, $v = 0 \leftarrow X^3\Sigma^-$, $v = 0$ rotational transitions were chosen from 27 possible (sub)branches (25) because they have splittings large enough to separate and identify the individual hyperfine components. The studied branches are given in Fig. 2, each for one arbitrary N. As can be seen, transitions to both Λ-doublet states in each of the three $^3\Pi_\Omega$ states, and from each of the three $^3\Sigma^-$ fine structure states $J = N + 1$, $J = N$, and $J = N - 1$ were induced. The parity of the levels is given by Dixon; in the $^3\Pi_0$ state, the Λ-doublets are inverted for $J' = 0$ to 7.

In theory, each rotational spectrum consists of 26 hyperfine components for the $\Delta J = 0$ branches and 22 for the $\Delta J = \pm 1$ branches, except for transitions involving $J = 0$ or 1. The signal-to-noise ratio of the strongest hyperfine lines varied between 20 at RC = 0.3 s in case of weakest rotational transitions and 100 for the strong $Q_i(N)$- and $R_i(N)$-branches from the lowest N states. To give an impression of the typical relative intensities and resolution, a measured spectrum of

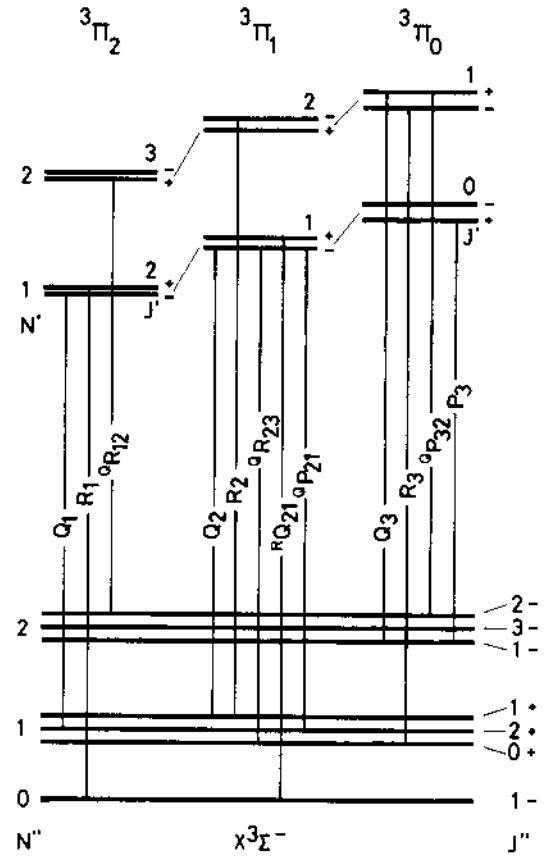

FIG. 2. Scheme of the investigated (sub)branches; for every branch at least one transition is measured.

the $P_3(3)$ transition is shown in Fig. 3. A particular spectrum was obtained for the $R_1(2)$ transition where several lines could not be assigned in first instance. It was found that these belonged to the $^RQ_{12}(1)$ transition, which overlaps completely with the $R_1(2)$ transition. Dixon's rotational assignment (10) was found to be correct for all 36 investigated rotational transitions. More than 300 hyperfine components were observed, and all of them could be assigned by a comparison with calculated splittings and relative intensities, starting with a trial set of hyperfine constants. The observed hyperfine splittings (Appendix B) are measured relative to the strongest components, which for all cases is the transition $F'' = J'' + 3/2 \rightarrow F' = J' + 3/2$. The experimental error is taken as one standard deviation from at least four measurements of each line, rounded off to 0.5 MHz, with a minimum of 2.0 MHz for the strong components. For the weaker components and the lines with small overlap, the experimental error was increased to a maximum of 6.0 MHz. Out of all the measured lines, 296 splittings without severe overlap were included in the input data set for the computer fitting program. For reasons of convergence, the magnetic hyperfine interaction constants were obtained as linear combinations a, $a + b + c$, b, and d for the $A^3\Pi$ state and $b + c/3$ and c for the $X^3\Sigma^-$ state. The resulting values from the least squares fit for all hyperfine constants for ground and excited states are listed in Table 2. The agreement between the measured and calculated splittings is very good (see Appendix B). Also, the relative intensities of the measured and calculated spectra are in close agreement, as can be seen from Fig. 3 for the $P_3(3)$ transition. A similar calculation using a rotational matrix without the Λ-doubling and spin–spin interactions for the $A^3\Pi$ state resulted in constants that agreed within the error limits as given in Table 2. The largest change by the exclusion of Λ-doubling and spin–spin interaction was obtained for the a constants and turned out to be smaller than 3%. The $b_{N,H}$ and $c_{N,H}$ constants for the ground state are in good agreement with the values obtained by Van den Heuvel *et al.* (20). In Fig. 4 the hyperfine level structure, as calculated from the experimental constants, is shown as a function of the J quantum number for the six $^3\Pi_\Omega$ upper and lower Λ-doublet states and the three $X^3\Sigma$ fine structure states. The hyperfine levels with $F = J \pm 3/2$ are uniquely defined, for $F = J \pm 1/2$ there are two levels, because of two nuclear spins; these levels are indicated with an extra label 1 for upper and 2 for lower energy.

TABLE 2. Hyperfine constants for the $A^3\Pi$ and $X^3\Sigma^-$, $v = 0$ states of the NH molecule (in megahertz). The subscripts N and H refer to the nitrogen and hydrogen nucleus

	$A^3\Pi$	$X^3\Sigma$
a_N	89.6±2.3	
b_N	153.6±0.4	41.7±0.5
c_N	15.2±2.6	−66.3±0.6
d_N	66.4±0.4	
$b_N + c_N/3$	158.7±0.9	19.6±0.4
a_H	74.1±1.5	
b_H	270.8±0.6	−96.5±1.4
c_H	90.5±4.5	90.6±1.9
d_H	26.0±0.6	
$b_H + c_H/3$	301.0±1.6	−66.3±1.2
eQq_1	7.1±1.5	−5.0±1.2
eQq_2	21.9±2.4	

Unfortunately no complete *ab initio* calculations exist for the hyperfine structure of NH. Some qualitative physical information can be deduced from the measured constants by interpreting them as expectation values of electron densities. In the spectroscopic approximation (26), the formulas can be rewritten as averaged electron densities (33),

$$a_k = \zeta_k \left\langle \frac{1}{r_k^3} \right\rangle_\pi$$

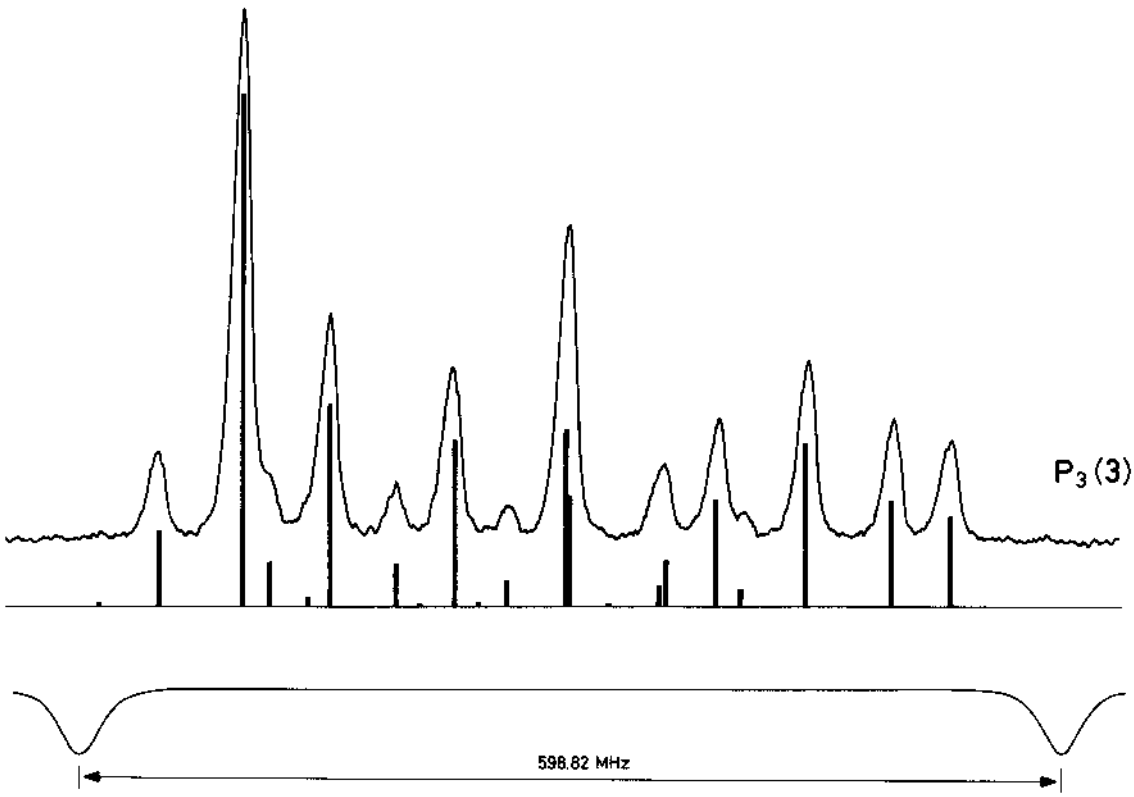

FIG. 3. Observed and calculated spectrum of the $P_3(3)$ transition.

$$b_{F,k} = \frac{8}{3}\pi\zeta_k\langle\psi^2(0_k)\rangle_{\sigma,\pi}$$

$$c_k = \frac{3}{2}\zeta_k\left\langle\frac{3\cos^2\theta_k - 1}{r_k^3}\right\rangle_{\sigma,\pi}$$

$$d_k = \frac{3}{2}\zeta_k\left\langle\frac{\sin^2\theta_k}{r_k^3}e^{-2i\phi_k}\right\rangle_{\pi}$$

$$q_1 = \frac{2}{R} - \left\langle\frac{3\cos^2\theta_{1N} - 1}{r_{1N}^3}\right\rangle_{T}$$

$$q_2 = -3\left\langle\frac{\sin^2\theta_{1N}}{r_{1N}^3}e^{-2i\phi_{1N}}\right\rangle_{T}$$

where the subscripts π and σ refer to the open-shell π and σ electrons while T denotes contributions from all electrons. In the expressions for q_2 and d_k, the averages are taken between electron distributions with $\Delta\Lambda = \pm 2$, $\Delta\Sigma = 0$, and $\Delta\Lambda = \pm 2$, $\Delta\Sigma = \mp 1$, respectively. The spectroscopic approximation assumes that the contribution of closed-shell electrons to the constants a, b, c, and d cancels because $\sum_i l_i = 0$ and $\sum_i s_i = 0$ for each closed shell, and the averages should be taken over open-shell electrons. In the $X^3\Sigma$ ground state, the electronic configuration is $(1s\sigma)^2(2s\sigma)^2(2p\sigma)^2(2p\pi)^2$ and in the $A^3\Pi$ state one closed-shell $2p\sigma$ electron is excited to a $2p\pi$ orbital, resulting in a configuration $(1s\sigma)^2(2s\sigma)^2(2p\sigma)(2p\pi)^3$. The situation in NH with the four open-shell electrons is more complex than the case of $^2\Pi$ states with three π electrons in the outer shell, such as the ground electronic states of OH and SH (33) and IO (34). We did not use a general subscript u for unpaired electrons at this stage, because in the spectroscopic approximation there are two unpaired electrons, one π and one σ, that contribute in a different way to the hyperfine constants. Only electrons with a nonzero orbital angular momentum, thus π electrons, contribute to the constant a and hence to $\langle 1/r^3\rangle$ because a refers to the $\boldsymbol{l}\cdot\boldsymbol{L}$ interaction. The constants d and q_2 originate from $|\Delta\Lambda| = 2$ matrix elements and this also can be caused only by π electrons. In Table 3 the calculated expectation values around the nitrogen and hydrogen nuclei are listed for both electronic states. In this calculation the magnetic g factors, $g_H = 5.585$ and $g_N = 0.40365$, as well as the quadrupole moment of the nitrogen nucleus $Q_N = 2.66\cdot 10^{-49}$ C m^2 were taken from the literature (35).

A first conclusion that can be drawn from the large values of $\langle 1/r^3\rangle\,\pi$ and $\langle \sin^2\theta/r^3\rangle\,\pi$ with respect to the nitrogen nucleus, in comparison with the values related

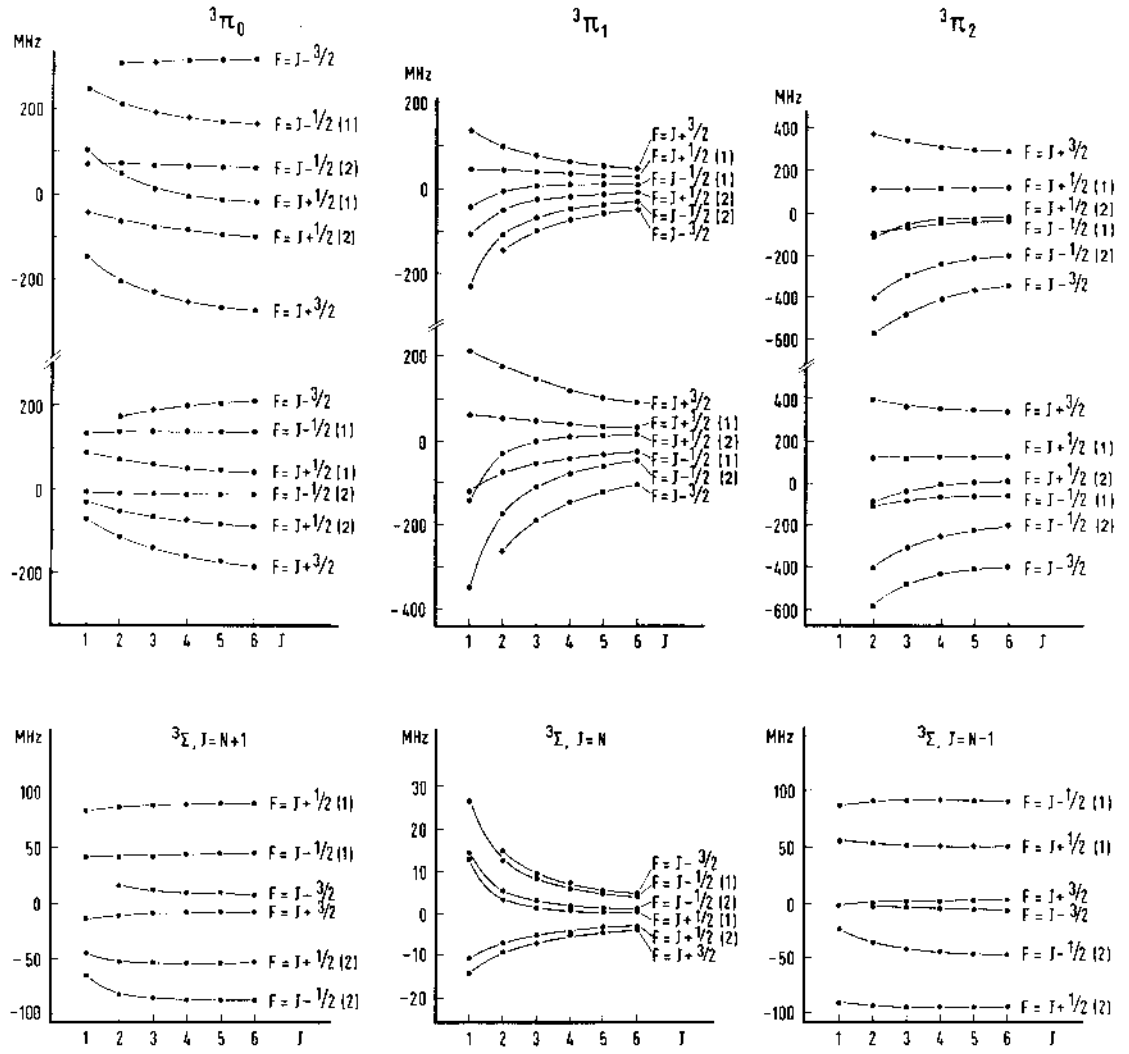

FIG. 4. Scheme of the hyperfine structure of the $A^3\Pi$ (upper and lower Λ-doublet states) and the $X^3\Sigma^-$ states of NH as a function of the J quantum number and calculated from the experimental hyperfine constants; levels with the same F quantum number have been denoted by an additional index (1) and (2) for upper and lower energy respectively.

to the hydrogen nucleus, is that in the $A^3\Pi$ state the three π orbitals are located mainly on the nitrogen nucleus. It follows that in the spectroscopic approximation the bonding will be due to the $2p\sigma$ orbital. This corresponds to the model given by Herzberg (25) in which he ascribes the stability of the $X^3\Sigma^-$ ground state to a mixing of a $2p\sigma$ orbital located on the nitrogen nucleus and the $1s\sigma$ orbital of the hydrogen atom when the two atoms are brought together, resulting in a bonding and an antibonding orbital. In this model, the electron in the antibonding orbital will be excited to the $2p\pi$ shell in a transition to the $A^3\Pi$ state.

Because of the fact that π-electron clouds have a nodal plane on the internuclear axis, they do not contribute to the Fermi-contact terms, which are proportional to $\langle\psi^2(0)\rangle$. Hence in the spectroscopic approximation, only the unpaired σ orbital gives a contribution and this explains why the Fermi-contact terms are much larger in the $A^3\Pi$ state than in the ground state. Similar arguments seem to apply to the OH and SH molecule to explain relative values of the Fermi-contact terms in the $X^2\Pi$ ground (33) and $A^2\Sigma^+$ excited states (2, 3). The Fermi-contact terms in the $X^3\Sigma^-$ ground state are probably due to polarization effects that cannot be explained within the spectroscopic approximation. In a valence configuration interaction calculation (28), it was found that the spin density at the nitrogen nucleus is twice that at the proton for an internuclear distance $R = 1.96\ a_0$ (12). However, this calculation does not produce a significant difference in spin density between the $A^3\Pi$ and

TABLE 3. Averaged electron densities around both nuclei, N and H, in the $A^3\Pi$ and $X^3\Sigma^-$ states of NH (in units of 10^{30} m^{-3})

	$A^3\Pi$		$X^3\Sigma^-$	
	N	*H*	*N*	*H*
$\left\langle \frac{1}{r^3} \right\rangle_\pi$	14.4(4)	0.94(5)		
$\left\langle \frac{\sin^2\theta}{r^3} \right\rangle_\pi$	7.11(4)	0.219(6)		
$\left\langle \frac{3\cos^2\theta - 1}{r^3} \right\rangle_{\pi,\sigma}$	1.63(18)	0.76(3)	−7.09(7)	0.77(2)
$\langle\psi^2(0)\rangle_{\pi,\sigma}$	3.04(2)	0.45(2)	0.375(8)	−0.100(2)
$\left\langle \frac{3\cos^2\theta - 1}{r^3} \right\rangle_T$	−10.2(23)		10.8(27)	
$\left\langle \frac{\sin^2\theta}{r_{1N}^3} \right\rangle_T$	12.7(15)			

$X^3\Sigma$ states, which shows that exact calculation of hyperfine constants is a delicate matter.

At first glance the values of $\langle \sin^2\theta_N/r_{1N}^3\rangle_\pi$ as calculated from the d_N and eQq_2 constants and formulas (14), are opposite in sign. In principle, the expectation value calculated from q_2, should be taken for all π electrons, but in the case of NH there are no inner shell π orbitals, so both values are averages over three π electrons. Following Bekooy *et al.* (34), the expectation value obtained from q_2 can be rewritten in an effective average over the *one unpaired* π electron, and in the case of three open-shell electrons, it can be replaced by $-\langle \sin^2\theta_N/r_{1N}^3\rangle_u$. The opposite holds for the expectation value as obtained from the d_N constant, it can be rewritten as $+\langle \sin^2\theta_N/r_{1N}^3\rangle_u$. The sign difference can be understood by expressing the electronic wave functions as Slater determinants (see Appendix A). Matrix elements corresponding to a change $|\Delta\Sigma| = 1$ of the total electron spin, as is the case for the *d* constants, produce an extra sign change because of a necessary permutation of the three π electrons in the Slater determinant. The values 7.11 ± 0.04 and 12.7 ± 1.5 obtained for $\langle \sin^2\theta_N/r_{1N}^3\rangle_u$ are in reasonable agreement, in view of the complex situation of two open shells where a breakdown of the spectroscopic approximation may be expected.

5. Conclusion

Laser induced fluorescence spectroscopy in a molecular beam has proved to be a powerful method for the investigation of the hyperfine structure of diatomic free radicals such as NH in the ground and excited electronic states. Because of the large tunability of a frequency doubled ring dye laser, spectra can be measured in a wide frequency range (295−340 nm).

From the large amount of data, the accuracy in the calculated hyperfine constants is comparable to the far infrared studies of the ground state. The effect of the quadrupole interaction in the $X^3\Sigma^-$ ground state of NH could be determined for the first time. For the determination of the hyperfine structure of the electronically excited states of free radicals, LIF in a molecular beam seems to be the best method at present. Possible improvements in the accuracy could be made in UV−microwave double resonance experiments in a molecular beam setup, as was shown already for the OH molecule (36).

The coaxial microwave cavity has shown to be an efficient source for NH radicals. We have found that they are not only produced in the $X^3\Sigma$ ground state, but also in the metastable $a^1\Delta$ state in a fraction of about 5% of the total NH production. From observed spectra of the $c^1\Pi \leftarrow a^1\Delta$ transition at $\lambda = 324$ nm, the hyperfine constants as well as the Λ-doubling parameters in the $a^1\Delta$ and $c^1\Pi$ states are derived (to be published). We hope that the determination of accurate hyperfine constants in several electronic states will be a stimulus for new *ab initio* calculations.

Acknowledgement

The authors wish to thank Dr. W. L. Meerts for helpful and stimulating discussions.

1. W. A. MAJEWSKI. Opt. Commun. **45**, 201 (1983).
2. J.J. TER MEULEN, W. A. MAJEWSKI, W. L. MEERTS, and A. DYMANUS. Chem. Phys. Lett. **94**, 225 (1983).
3. W. UBACHS, J. J. TER MEULEN, and A. DYMANUS. Chem. Phys. Lett. **101**, 1 (1983).

4. A. SCHADEE. Bull. Astron. Inst. Neth. **17**. 311 (1964).
5. J. L. SCHMITT. Publ. Astron. Soc. Pac. **81**, 657 (1969).
6. P. SWINGS, C. T. ELVEY, and H. W. BABCOCK. Astrophys. J. **94**, 320 (1941).
7. A. W. BREWER, P. A. DAVIS, and J. B. KERR. Nature (London), **270**. 35 (1972).
8. J. M. EDER. Denkschr. Wien. Akad. **60**, 1 (1893).
9. G. W. FUNKE. Z. Phys. **96**, 777 (1935); **101**, 104 (1936).
10. R. N. DIXON. Can. J. Phys. **37**, 1171 (1959).
11. M. H. HEBB. Phys. Rev. **49**, 610 (1936).
12. J. MALICET, J. BRION, and H. GUENEBAUT. J. Chem. Phys. Phys. Chim. Biol. **67**, 25 (1970).
13. G. H. DIEKE and R. W. BLUE. Phys. Rev. **45**, 395 (1934).
14. D. A. RAMSAY and P. J. SARRE. J. Mol. Spectrosc. **93**, 445 (1982).
15. R. W. LUNT, R. W. B. PEARSE, and E. C. W. SMITH. Proc. R. Soc. London Ser. A. **151**, 602 (1935).
16. W. R. M. GRAHAM and H. LEW. Can. J. Phys. **56**, 85 (1978).
17. A. GILLES, J. MASANET, and C. VERMEIL. Chem. Phys. Lett. **25**, 346 (1974).
18. P. F. BERNATH and T. AMANO. J. Mol. Spectrosc. **95**, 359 (1982).
19. F. D. WAYNE and H. E. RADFORD. Mol. Phys. **32**, 407 (1976).
20. F. C. VAN DEN HEUVEL, W. L. MEERTS, and A. DYMANUS. Chem. Phys. Lett. **92**, 215 (1982).
21. H. NEUHAUS. Z. Phys. **150**, 4 (1958).
22. L. Y. CHOW CHIU. Phys. Rev. **145**, 1 (1966).
23. R. H. GAMMON, R. C. STERN, M. E. LESK, B. G. WICKE, and W. KLEMPERER. J. Chem. Phys. **54**, 2136 (1970).
24. K. F. FREED. J. Chem. Phys. **45**, 4214 (1966).
25. G. HERZBERG. Spectra of diatomic molecules. D. Van Nostrand Company Inc., New York, NY. 1950.
26. R. A. FROSCH and H. M. FOLEY. Phys. Rev. **88**, 1337 (1952).
27. A. BANERJEE and F. GREIN. Chem. Phys. **35**, 119 (1978); W. H. HUO. J. Chem. Phys. **49**, 1482 (1968); P. J. HAY and T. H. DUNNING. J. Chem. Phys. **64**, 5077 (1976).
28. J. KOUBA and Y. ÖHRN. J. Chem. Phys. **52**, 538 (1970).
29. G. O. BRINK, R. A. FLUEGGE, and R. J. HULL. Rev. Sci. Instrum. **39**, 1171 (1968).
30. W. H. SMITH, J. BRZOZOWSKI, and P. ERMAN. J. Chem. Phys. **64**, 4268 (1976).
31. A. R. EDMONDS. Angular momentum in quantum mechanics. Princeton University Press, Princeton, NJ. 1957.
32. R. MCWEENY. J. Chem. Phys. **42**, 1717 (1965).
33. W. L. MEERTS and A. DYMANUS. Can. J. Phys. **53**, 2123 (1975).
34. J. P. BEKOOY, W. L. MEERTS, and A. DYMANUS. J. Mol. Spectrosc. **102**, 320 (1983).
35. C. M. LEDERER and V. S. SHIRLEY. Table of isotopes. 7th ed. John Wiley and Sons Inc., New York, NY. 1978.
36. J. J. TER MEULEN, W. UBACHS, and A. DYMANUS. *In* Laser spectroscopy VI. *Edited by* H. P. Weber and W. Lüthy. Springer Verlag, Berlin, FRG. 1983.
37. J. T. HOUGEN. J. Chem. Phys. **39**. 358 (1963).
38. I. KOPP and J. T. HOUGEN. Can. J. Phys. **45**, 2581 (1967).

Appendix A

The symmetry of the molecular wave function with respect to the reflection operation σ_{xz} is important since it fixes the signs of the hyperfine constants $d_{N,H}$ and q_2. In order to determine the symmetry of the electronic part of the wave function, we consider the effect of σ_{xz} on the electrons in the open shells. The molecular orbital (MO) configuration of NH in the $A^3\Pi$ state is $(1s\sigma)^2(2s\sigma)^2(2p\sigma)(2p\pi)^3$ and the wave function of the four open-shell electrons can be written as a Slater determinant, e.g.,

$$[A1] \quad |\Lambda = 1, \Sigma = 1\rangle = \{\sigma^+\pi_+^1\pi_+\pi_-^1\}$$

The upper signs correspond with $\sigma_i = \pm 1$ and the lower ones with $\lambda_i = \pm 1$, where σ_i and λ_i are the projections of the spin (s_i) and orbital (l_i) angular momentum of electron i on the internuclear axis. For $\Sigma = 0$ or -1 and $\Lambda = -1$, the wave functions and their relative phases are derived from [A1] by successive applications of the total electronic operators $\tilde{\mathbf{L}}_+ = \sum_i \tilde{\mathbf{l}}_{i+}$ and $\tilde{\mathbf{S}}_- = \sum_i \tilde{\mathbf{s}}_{i-}$ defined in the molecular frame of reference. For the single electron operators, the phase convention of Edwards (31) is used

$$[A2] \quad \begin{aligned} \tilde{\mathbf{l}}_{i\pm}|l_i\lambda_i\rangle &= \sqrt{(l_i \mp \lambda_i)(l_i \pm \lambda_i + 1)}\,|l_i\lambda_i \pm 1\rangle \\ \tilde{\mathbf{s}}_{i\pm}|s_i\sigma_i\rangle &= \sqrt{(s_i \mp \sigma_i)(s_i \pm \sigma_i + 1)}\,|s_i\sigma_i \pm 1\rangle \end{aligned}$$

where $|l_i\lambda_i\rangle$ and $|s_i\sigma_i\rangle$ are the orbital and spin part of the wave function of electron i.

As a result we obtain

$$[A3] \quad |\Lambda = -1, \Sigma = -1\rangle = \{\sigma^-\pi_-^-\pi_-^-\pi_-^1\}$$

Under a reflection in the plane containing the internuclear axis, $|l_i\lambda_i\rangle$ transforms as

$$[A4] \quad \sigma_{xz}|l_i\lambda_i\rangle = (-1)^{\lambda_i}|l_i\ -\lambda_i\rangle$$

where the phase factor originates from the relation

$$|l_i\lambda_i\rangle^* = (-1)^{\lambda_i}|l_i\ -\lambda_i\rangle$$

which is a direct consequence of the phase convention [A2]. From the transformation properties of the single-electron spin function as given by Hougen (37), it follows that

$$[A5] \quad \sigma_{xz}|s_i\sigma_i\rangle = (-1)^{s_i-\sigma_i}|s_i\ -\sigma_i\rangle$$

analogous to the symmetry of the total spin wave function (38). Application of σ_{xz} onto the wave function [A1] then gives

[A6] $$\sigma_{xz}|\Lambda = 1, \Sigma = 1\rangle = (-1)^{\Lambda-\Sigma}\{\sigma^-\pi_-^-\pi_-^+\pi_-^-\} = |\Lambda = -1, \Sigma = -1\rangle$$

Similarly for $\Sigma = 0$

[A7] $$\sigma_{xz}|\Lambda = 1, \Sigma = 0\rangle = -|\Lambda = -1, \Sigma = 0\rangle$$

The symmetry of the rotational part of the molecular wave function is given by (38)

[A8] $$\sigma_{xz}|J\,\Omega M_J\rangle = (-1)^{J-\Omega}|J\,-\Omega M_J\rangle$$

so that for the total wave function of NH in the $A^3\Pi$ state the result obtained is

[A9] $$\sigma_{xz}|\Lambda\Sigma\rangle|J\,\Omega M_J\rangle = (-1)^{\Lambda\ \Sigma}(-1)^{J-\Omega}|\ -\Lambda\ -\ \Sigma\rangle|J\ -\Omega M_J\rangle = (-1)^J|-\Lambda\ -\ \Sigma\rangle|J\ -\Omega M_J\rangle$$

which differs from the usually applied symmetry $(-1)^{J-S}$ that we obtain in the case of only one open-shell π electron.

The positive sign of the quadrupole coupling constant q_2 can be explained with help of Slater determinants:

$$q_2 = \frac{2\sqrt{6}}{e}\langle\Lambda = 1, \Sigma|T^{(2)}_{-2}(V_1)|\Lambda = -1, \Sigma\rangle$$

which (for $\Sigma = 1$) can be written as

[A10] $$q_2 = \frac{2\sqrt{6}}{e} \times \{\sigma^1\pi_+^1\pi_+\pi_-^-|T^{(2)}_{-2}(V_1)|\sigma^1\pi_-^-\pi_-^-\pi_-^1\} = \frac{2\sqrt{6}}{e}\langle\pi_1^-|T^{(2)}_2(V_1)|\pi^-\rangle = -3\langle\pi_+|C^{(2)}_2(\theta_{1N}, \phi_{1N})/r^3_{1N}|\pi_-\rangle = +3\left\langle\frac{\sin^2\theta_{1N}}{r^3_{1N}}\right\rangle_u$$

where the integration over the azimuthal angle ϕ gives a negative sign. This is also the case for the $d_{N,H}$ constants, but an additional negative sign is obtained owing to an odd permutation of the single-electron wave functions in one of the Slater determinants. The d constants are proportional to matrix elements of the type

$$\langle\Lambda = 1, \Sigma|T^{(1)}_{-1}(s_1)C^{(2)}_2(\theta_{1k}, \phi_{1k})/r^3_{1k}|\ \Lambda = -1, \Sigma + 1\rangle$$

which can be rewritten with (for $\Sigma = -1$)

$$|\Lambda = 1, \Sigma = -1\rangle = \{\sigma^-\pi_1^+\pi_1^-\pi^-\}$$

and

$$|\Lambda = -1, \Sigma = 0\rangle = \frac{1}{\sqrt{2}}[\{\sigma^+\pi_-^-\pi_-^-\pi_1^-\} + \{\sigma^-\pi_-^-\pi^+\pi^-\}]$$

as

$$\frac{1}{\sqrt{2}}\{\sigma^-\pi_-^-\pi_-^-\pi^-|T^{(1)}_{-1}(s_1)C^{(2)}_2(\theta_{1k}, \phi_{1k})/r^3_{1k}|\sigma\ \ \pi_-\pi_-^1\pi_-^-\} = -\frac{1}{\sqrt{2}}\langle\pi_1^-|T^{(1)}_1(s_1)C^{(2)}_2(\theta_{1k}, \phi_{1k})/r^3_{1K}|\pi^+\rangle = -\frac{1}{2}\langle\pi_+^-|C^{(2)}_2(\theta_{1k}, \phi_{1k})/r^3_{1k}|\pi_-^+\rangle = +\frac{1}{4}\sqrt{3/2}\left\langle\frac{\sin^2\theta_{1k}}{r^3_{1k}}\right\rangle_u$$

Appendix B[a]

F" → F'	Obs. Freq.	Obs-Calc.	F" → F'	Obs. Freq.	Obs-Calc.
Transition $Q_1(1)$			$7/2_1 \rightarrow 7/2_2$	−487.8 ± 2.0	−0.3
$5/2_2 \rightarrow 7/2$	40.7 ± 2.0	−1.0	$5/2_2 \rightarrow 5/2_2$	−551.9 ± 5.0	−2.1
$5/2_1 \rightarrow 7/2$	−95.2 ± 2.5	0.8	$7/2_2 \rightarrow 5/2_2$	−582.5 ± 3.0	−2.4
$3/2_2 \rightarrow 5/2_1$	−189.6 ± 3.0	−0.9	$3/2 \rightarrow 5/2_2$	−648.9 ± 2.0	−2.7
$5/2_2 \rightarrow 3/2_1$	−216.2 ± 2.5	−0.9	$5/2_1 \rightarrow 5/2_2$	−679.7 ± 2.0	−4.3
$7/2 \rightarrow 5/2_1$	−255.6 ± 4.0	1.4	$5/2_2 \rightarrow 3/2_2$	−721.9	
$5/2_1 \rightarrow 5/2_1$	−351.5 ± 2.5	1.5	$7/2_1 \rightarrow 5/2_2$		
$3/2_2 \rightarrow 3/2_1$	−408.4 ± 2.0	0.1	$3/2 \rightarrow 3/2$	−817.7 ± 3.0	−3.9
$5/2_2 \rightarrow 3/2_1$	−435.1 ± 4.0	0.0	$5/2_1 \rightarrow 3/2$	−846.7 ± 3.5	−3.7
$5/2_2 \rightarrow 5/2_2$	−444.5 ± 4.0	1.5	Transition $Q_1(3)$		
$7/2 \rightarrow 5/2_2$	−486.3 ± 2.0	1.5	$9/2_2 \rightarrow 11/2$	43.3 ± 2.5	−0.5
$3/2_1 \rightarrow 3/2_1$	−528.6 ± 4.0	0.3	$9/2_1 \rightarrow 11/2$	−97.5 ± 3.0	−0.9
$3/2_1 \rightarrow 5/2_2$	−538.5 ± 4.0	1.4	$7/2_2 \rightarrow 9/2_1$	−116.3 ± 2.5	0.2
$5/2_1 \rightarrow 5/2_2$	−582.0 ± 2.0	1.7	$9/2_2 \rightarrow 9/2_1$	−149.8 ± 2.0	−1.0
$5/2_2 \rightarrow 3/2_2$	−734.9 ± 2.5	2.4	$11/2 \rightarrow 9/2_1$	−192.6 ± 3.0	0.0
$1/2 \rightarrow 3/2_2$	−804.7 ± 2.5	1.0	$7/2_2 \rightarrow 7/2_1$	−290.3 ± 6.0	−1.2
$3/2_1 \rightarrow 3/2_2$	−829.8 ± 2.0	0.4	$9/2_2 \rightarrow 7/2_1$	−323.1 ± 4.0	−1.7
$5/2_1 \rightarrow 3/2_2$	−873.3		$11/2 \rightarrow 9/2_2$	−349.8 ± 2.5	−0.1
$3/2_2 \rightarrow 1/2$			$7/2_1 \rightarrow 9/2_2$	−402.7 ± 3.0	−0.9
$1/2 \rightarrow 1/2$	−975.8 ± 2.5	0.3	$7/2_1 \rightarrow 7/2_1$	−420.7 ± 6.0	−3.4
$3/2_1 \rightarrow 1/2$	−1000.9 ± 2.5	−0.3	$9/2_1 \rightarrow 9/2_2$	−447.5 ± 2.0	−1.2
Transition $Q_1(2)$			$7/2_2 \rightarrow 7/2_2$	−475.3 ± 5.0	−0.1
$7/2_2 \rightarrow 9/2$	40.8 ± 3.0	−2.5	$9/2_2 \rightarrow 7/2_2$	−508.6 ± 2.5	−1.0
$7/2_1 \rightarrow 9/2$	−95.6 ± 3.0	0.8	$5/2 \rightarrow 7/2_2$	−572.8 ± 3.0	−1.0
$5/2_2 \rightarrow 7/2_1$	−141.2 ± 3.0	1.6	$7/2_1 \rightarrow 7/2_2$	−605.4 ± 3.0	−1.9
$7/2_2 \rightarrow 7/2_1$	−172.3 ± 2.0	0.7	$7/2_2 \rightarrow 5/2$	−639.0 ± 6.0	−1.6
$7/2_1 \rightarrow 7/2_1$	−311.7		$9/2_1 \rightarrow 7/2_2$	−649.5 ± 6.0	−1.5
$5/2_2 \rightarrow 7/2_2$			$5/2_2 \rightarrow 5/2$	−731.7 ± 3.5	−2.7
$5/2_2 \rightarrow 5/2_1$	−331.0 ± 3.0	−0.4	$7/2_1 \rightarrow 5/2$	−769.2 ± 4.0	−3.5
$7/2_2 \rightarrow 7/2_2$	−345.9 ± 6.0	1.9	Transition $R_1(0)$		
$7/2_2 \rightarrow 5/2_1$	−361.7 ± 6.0	−0.8	$3/2_2 \rightarrow 5/2_1$	−234.4 ± 3.0	−0.2
$9/2 \rightarrow 7/2_2$	−390.3 ± 2.0	0.8	$5/2 \rightarrow 5/2_1$	−267.8 ± 4.5	0.8
$5/2_1 \rightarrow 7/2_2$	−443.2 ± 4.0	−0.1	$3/2_1 \rightarrow 5/2_1$	−362.6 ± 2.0	0.6
$5/2_1 \rightarrow 5/2_1$	−457.5 ± 4.0	−1.3	$1/2_2 \rightarrow 3/2_1$	−443.5 ± 6.0	1.2

APPENDIX B. (*Continued*)

F" → F'	Obs. Freq.	Obs-Calc.	F" → F'	Obs. Freq.	Obs-Calc.
$1/2_2 \rightarrow 3/2_1$	−462.7		Transition $R_1(4)$		
$1/2_2 \rightarrow 5/2_2$			$11/2_2 \rightarrow 13/2_1$	−172.2 ± 2.0	0.1
$5/2 \rightarrow 3/2_1$	−496.9		$13/2 \rightarrow 13/2_1$	−216.6 ± 3.0	−0.4
$5/2 \rightarrow 5/2_2$			$11/2_2 \rightarrow 13/2_2$	−290.5 ± 3.5	−0.8
$1/2_1 \rightarrow 3/2_1$	−552.4 ± 3.5	−0.1	$9/2_2 \rightarrow 11/2_1$	−327.6 ± 2.0	1.7
$3/2_1 \rightarrow 3/2_1$	−591.5		$11/2_2 \rightarrow 11/2_1$	−360.8 ± 4.0	2.2
$3/2_1 \rightarrow 5/2_2$			$11/2_1 \rightarrow 13/2_2$	−431.5 ± 2.5	−1.2
$1/2_2 \rightarrow 3/2_2$	−766.6 ± 2.5	0.1	$9/2_2 \rightarrow 11/2_2$	−475.5 ± 4.0	2.3
$5/2 \rightarrow 3/2_2$	−800.3 ± 3.5	0.5	$11/2_2 \rightarrow 11/2_2$	−512.6 ± 6.0	−1.1
$1/2_1 \rightarrow 3/2_2$	−857.1 ± 2.5	−1.7	$9/2_1 \rightarrow 11/2_2$	−608.3 ± 4.5	−0.6
$3/2_1 \rightarrow 3/2_2$	−896.1 ± 2.0	−0.6	$11/2_1 \rightarrow 11/2_2$	−655.1	
$1/2_2 \rightarrow 1/2$	−923.7 ± 3.0	−1.5	$9/2_2 \rightarrow 9/2$		
$1/2_2 \rightarrow 1/2$	−941.8 ± 3.5	−0.8	$7/2_2 \rightarrow 9/2$	−756.3 ± 5.0	1.6
$1/2_1 \rightarrow 1/2$	−1031.9 ± 2.0	−2.0	$9/2_1 \rightarrow 9/2$	−789.6 ± 6.0	1.5
$3/2_1 \rightarrow 1/2$	−1071.5 ± 2.5	−1.6	Transition $R_1(5)$		
Transition $R_1(2)$			$13/2_2 \rightarrow 15/2_1$	−167.0 ± 2.5	1.6
$7/2_2 \rightarrow 9/2_1$	−187.1 ± 3.0	−1.6	$13/2_2 \rightarrow 15/2_2$	−280.0 ± 3.5	1.1
$9/2 \rightarrow 9/2_1$	−230.7 ± 3.5	−1.9	$11/2_2 \rightarrow 13/2_1$	−317.7	
$5/2_1 \rightarrow 7/2_2$	−658.6 ± 3.0	0.6	$13/2_1 \rightarrow 15/2_1$		
$3/2 \rightarrow 5/2$	−810.1 ± 2.5	1.4	$13/2_1 \rightarrow 15/2_2$	−422.5 ± 2.0	−0.7
$5/2_1 \rightarrow 5/2$	−839.1 ± 3.5	1.6	$11/2_1 \rightarrow 13/2_1$	−455.0 ± 6.0	−0.7
Transition $R_1(3)$			$13/2_1 \rightarrow 13/2_1$	−495.5 ± 4.0	3.2
$9/2_2 \rightarrow 11/2_1$	−178.2 ± 2.5	−0.7	$11/2_1 \rightarrow 13/2_2$	−592.1 ± 2.5	2.2
$11/2_2 \rightarrow 11/2_1$	−221.8 ± 3.5	−0.6	$13/2_1 \rightarrow 13/2_2$	−638.2 ± 6.0	0.4
$9/2_2 \rightarrow 11/2_2$	−303.0 ± 5.0	−0.3	$9/2 \rightarrow 11/2$	−738.6 ± 4.0	5.3
$9/2_1 \rightarrow 11/2_1$	−318.1 ± 5.0	−0.3	$11/2_1 \rightarrow 11/2$	−774.0 ± 2.0	4.3
$7/2_2 \rightarrow 9/2_1$	−338.6 ± 3.5	−0.6	Transition $R_1(6)$		
$9/2_2 \rightarrow 9/2_1$	−369.5 ± 5.0	0.9	$15/2_2 \rightarrow 17/2_1$	−164.8 ± 2.0	1.0
$9/2_1 \rightarrow 11/2_2$	−442.5 ± 3.5	0.6	$15/2_2 \rightarrow 17/2_2$	−274.7 ± 3.5	0.2
$7/2_2 \rightarrow 9/2_2$	−498.1 ± 5.0	1.0	$13/2_2 \rightarrow 15/2_1$	−314.4 ± 3.0	4.6
$9/2_2 \rightarrow 9/2_2$	−531.0 ± 5.0	0.5	$15/2_1 \rightarrow 17/2_2$	−415.6 ± 3.0	0.1
$7/2_1 \rightarrow 9/2_2$	−625.9 ± 3.5	1.5	$13/2_2 \rightarrow 15/2_2$	−447.0	
$9/2_1 \rightarrow 9/2_2$	−672.4 ± 5.0	−0.5	$13/2_1 \rightarrow 15/2_1$		
$5/2 \rightarrow 7/2$	−775.8 ± 4.5	2.6	$15/2_2 \rightarrow 15/2_2$	−486.3 ± 5.0	1.8
$7/2_1 \rightarrow 7/2$	−807.9 ± 5.0	2.2	$13/2_1 \rightarrow 15/2_2$	−582.2 ± 3.0	2.4

APPENDIX B. (*Continued*)

F" → F'	Obs. Freq.	Obs.-Calc.	F" → F'	Obs. Freq.	Obs.-Calc.
$15/2_1 \rightarrow 15/2_2$	−627.9 ± 5.0	1.0	$3/2 \rightarrow 3/2_2$	−354.9 ± 5.0	0.0
$11/2 \rightarrow 13/2$	−727.9 ± 3.5	5.9	$3/2 \rightarrow 1/2_2$	−560.6 ± 6.0	0.0
$13/2_1 \rightarrow 13/2$	−763.5 ± 5.0	5.4	Transition $^{Q}R_{23}(2)$		
Transition $R_1(7)$			$3/2_2 \rightarrow 5/2_1$	−32.9 ± 2.0	0.5
$17/2_2 \rightarrow 17/2_1$	−161.1 ± 2.0	2.5	$3/2_2 \rightarrow 5/2_2$	−117.9	
$15/2_2 \rightarrow 17/2_1$	−308.1		$5/2_2 \rightarrow 5/2_1$		
$19/2 \rightarrow 17/2_2$			$3/2_1 \rightarrow 5/2_1$	−179.9 ± 2.0	−1.6
$17/2_1 \rightarrow 17/2_2$	−410.0 ± 3.5	1.1	$5/2_2 \rightarrow 5/2_2$	−207.1 ± 2.5	−0.3
$15/2_1 \rightarrow 17/2_2$	−574.6 ± 4.5	2.6	$1/2_2 \rightarrow 3/2_1$	−228.1 ± 3.0	−2.2
$13/2 \rightarrow 15/2$	−719.5 ± 6.0	6.7	$3/2_1 \rightarrow 5/2_2$	−264.4	
Transition $^{Q}R_{12}(3)$			$3/2_2 \rightarrow 3/2_2$		
$7/2_1 \rightarrow 9/2_1$	−198.3 ± 2.5	1.4	$3/2_1 \rightarrow 3/2_1$	−309.1 ± 6.0	−3.6
$7/2_2 \rightarrow 9/2_2$	−349.8 ± 3.0	1.5	$1/2_2 \rightarrow 3/2_2$	−339.7	
$5/2_1 \rightarrow 7/2_1$	−378.8 ± 3.0	1.3	$1/2_1 \rightarrow 3/2_1$		
$5/2_2 \rightarrow 7/2_2$	−558.4 ± 3.5	1.6	$1/2_2 \rightarrow 1/2$	−414.4	
$3/2_2 \rightarrow 5/2$	−727.2 ± 5.0	2.9	$3/2_1 \rightarrow 3/2_2$		
Transition $Q_2(1)$			Transition $^{R}Q_{21}(4)$		
$3/2_1 \rightarrow 5/2$	−26.2 ± 3.0	0.0	$9/2_2 \rightarrow 9/2_1$	36.4 ± 3.0	3.4
$5/2 \rightarrow 3/2_1$	−149.4 ± 3.5	−1.2	$11/2_2 \rightarrow 11/2_1$	20.5 ± 3.0	1.3
$1/2_1 \rightarrow 3/2_1$	−173.6		$7/2 \rightarrow 7/2$	−126.2 ± 3.5	5.0
$1/2_2 \rightarrow 3/2_1$			$9/2_1 \rightarrow 9/2_2$	−143.3 ± 3.5	1.9
$3/2_2 \rightarrow 1/2_1$	−336.2 ± 5.5	−1.8	$11/2_1 \rightarrow 11/2_2$	−164.0 ± 4.0	0.4
$1/2_2 \rightarrow 3/2_2$	−381.1		Transition $^{R}Q_{21}(5)$		
$3/2_1 \rightarrow 3/2_2$			$11/2_2 \rightarrow 11/2_1$	43.8 ± 3.0	2.6
$1/2_1 \rightarrow 3/2_2$	−393.2 ± 5.0	−0.5	$13/2_2 \rightarrow 13/2_1$	22.8 ± 4.5	−0.3
$3/2_2 \rightarrow 1/2_2$	−562.5 ± 4.5	1.7	$9/2 \rightarrow 9/2$	−108.5 ± 3.0	4.6
$1/2_2 \rightarrow 1/2_2$	−586.7		$11/2_1 \rightarrow 11/2_2$	−130.0 ± 4.0	1.2
$3/2_1 \rightarrow 1/2_2$			$13/2_1 \rightarrow 13/2_2$	−153.1 ± 3.0	1.2
Transition $R_2(3)$			Transition $^{R}Q_{21}(6)$		
$7/2_1 \rightarrow 9/2_1$	−37.5 ± 2.0	0.0	$13/2_2 \rightarrow 13/2_1$	50.7 ± 3.5	3.7
$5/2_2 \rightarrow 7/2_2$	−121.5 ± 2.0	0.5	$15/2_2 \rightarrow 15/2_1$	27.0 ± 3.5	1.1
$3/2_2 \rightarrow 5/2$	−151.4 ± 2.5	2.2	$11/2 \rightarrow 11/2$	−96.2 ± 4.0	3.6
Transition $^{Q}R_{23}(1)$			$13/2_1 \rightarrow 13/2_2$	−120.4 ± 3.5	0.5
$3/2 \rightarrow 3/2_1$	−147.0 ± 2.0	1.2	$15/2_1 \rightarrow 15/2_2$	−147.2 ± 3.5	−0.4
$3/2 \rightarrow 1/2_1$	−335.0 ± 5.0	−4.2			

APPENDIX B. (*Continued*)

F" → F'	Obs. Freq.	Obs.-Calc.	F" → F'	Obs. Freq.	Obs.-Calc.
Transition $^{Q}P_{21}(1)$			$7/2_2 \rightarrow 7/2_1$	294.3 ± 3.0	-1.7
$5/2_2 \rightarrow 5/2$	40.9 ± 2.5	-0.8	$5/2_2 \rightarrow 5/2_1$	329.0 ± 5.0	-0.2
$3/2_2 \rightarrow 3/2_1$	-80.6 ± 3.0	-0.7	$3/2 \rightarrow 3/2$	339.4 ± 5.0	-1.0
$5/2_2 \rightarrow 3/2_1$	-107.8 ± 5.0	-1.3	$5/2_2 \rightarrow 3/2$ } 377.5		
$5/2_1 \rightarrow 3/2_1$	-242.9 ± 2.0	1.3	$7/2_2 \rightarrow 5/2_1$ }		
$3/2_2 \rightarrow 1/2_1$ } -267.4			Transition $Q_3(5)$		
$3/2_2 \rightarrow 3/2_2$ }			$9/2_1 \rightarrow 11/2$	-46.6 ± 3.0	0.2
$5/2_2 \rightarrow 3/2_2$	-314.7 ± 3.0	-1.5	$9/2_1 \rightarrow 9/2$	42.0 ± 2.5	0.2
$1/2 \rightarrow 3/2_2$ } -388.4			$7/2_1 \rightarrow 7/2$	65.2 ± 2.0	0.3
$3/2_1 \rightarrow 1/2_1$ }			$11/2_2 \rightarrow 9/2$	88.6 ± 6.0	-0.1
$3/2_1 \rightarrow 3/2_2$	-409.5 ± 3.5	-2.5	$9/2_2 \rightarrow 11/2$ } 104.5		
$5/2_1 \rightarrow 3/2_2$	-452.0 ± 4.0	-1.1	$9/2_1 \rightarrow 7/2_2$ }		
$3/2_2 \rightarrow 1/2_2$	-494.4 ± 6.0	-2.1	$7/2_1 \rightarrow 5/2$ } 256.3		
$1/2 \rightarrow 1/2_2$	-590.1 ± 6.0	-1.9	$7/2_2 \rightarrow 9/2_1$ }		
$3/2_1 \rightarrow 1/2_2$	-615.0 ± 6.0	-2.3	$9/2_2 \rightarrow 9/2_1$	305.8 ± 5.0	-0.4
Transition $^{Q}P_{21}(2)$			$7/2_2 \rightarrow 7/2_1$	349.0 ± 5.0	-0.7
$7/2_2 \rightarrow 7/2$	41.8 ± 4.0	-1.5	$5/2 \rightarrow 5/2_2$	369.1 ± 5.0	-0.8
$7/2_2 \rightarrow 5/2_1$	-78.9 ± 2.0	-0.4	$9/2_2 \rightarrow 7/2_1$	396.4 ± 6.0	-0.9
$7/2_2 \rightarrow 5/2_2$	-163.5 ± 6.0	0.0	$7/2_2 \rightarrow 5/2$	409.1 ± 6.0	-1.2
$5/2_2 \rightarrow 3/2_1$	-176.6 ± 6.0	-1.2	Transition $Q_3(6)$		
$7/2_1 \rightarrow 5/2_1$	-218.0 ± 2.0	0.2	$11/2_1 \rightarrow 11/2_2$	50.2 ± 2.0	0.9
$5/2_1 \rightarrow 5/2_2$	-258.7 ± 4.0	0.1	$9/2_1 \rightarrow 9/2_2$	79.8 ± 2.0	1.4
$3/2 \rightarrow 3/2_1$	-277.7 ± 6.0	-5.9	$9/2_2 \rightarrow 11/2_1$	270.7 ± 6.0	3.6
$5/2_1 \rightarrow 3/2_1$ } -303.3			$11/2_2 \rightarrow 11/2_1$	315.9 ± 2.5	2.7
$7/2_1 \rightarrow 5/2_2$ }			$9/2_2 \rightarrow 9/2_1$	366.7 ± 3.0	2.8
$3/2 \rightarrow 3/2_2$	-374.4 ± 4.0	0.0	$7/2 \rightarrow 7/2$	394.1 ± 3.0	3.3
$5/2_1 \rightarrow 3/2_2$	-404.4 ± 3.0	-0.7	Transition $Q_3(7)$		
$3/2 \rightarrow 1/2$	-461.7 ± 3.0	-0.2	$13/2_1 \rightarrow 15/2$	-43.5 ± 3.0	1.3
Transition $Q_3(4)$			$13/2_1 \rightarrow 13/2_2$	55.5 ± 2.0	0.8
$7/2_1 \rightarrow 9/2$	-48.5 ± 2.5	0.0	$11/2_1 \rightarrow 11/2_2$	89.5 ± 2.0	1.0
$7/2_1 \rightarrow 7/2_2$	31.0 ± 3.0	-0.1	$15/2 \rightarrow 13/2_1$ } 225.1		
$5/2_1 \rightarrow 5/2_2$	45.8 ± 3.0	-0.4	$11/2_2 \rightarrow 11/2_1$ }		
$7/2_2 \rightarrow 7/2_2$	174.3 ± 3.0	0.1	$13/2_2 \rightarrow 13/2_1$	319.6 ± 3.0	1.1
$9/2 \rightarrow 7/2_1$	200.5 ± 3.0	-0.9	$11/2_2 \rightarrow 11/2_1$	377.1 ± 3.0	2.8
$5/2_1 \rightarrow 3/2_2$	244.8 ± 6.0	-1.2	$9/2 \rightarrow 9/2$	408.5 ± 3.0	2.1

APPENDIX B. (*Continued*)

F" → F'	Obs. Freq.	Obs-Calc.	F" → F'	Obs. Freq.	Obs-Calc.
$11/2_2 \rightarrow 9/2$	447.8 ± 3.5	-0.3	$7/2_1 \rightarrow 9/2_1$	210.1 ± 5.0	3.1
Transition $R_3(1)$			$5/2_1 \rightarrow 7/2_2$	234.6 ± 2.5	1.7
$3/2 \rightarrow 3/2_2$	106.1 ± 2.0	1.0	$7/2_2 \rightarrow 9/2_2$	261.9 ± 5.0	-2.1
$3/2 \rightarrow 1/2_2$	218.4 ± 2.0	-0.8	$7/2_2 \rightarrow 9/2_1$	350.5 ± 2.0	0.4
$3/2 \rightarrow 3/2_1$	250.9 ± 2.0	0.2	$7/2_1 \rightarrow 7/2_1$	386.9 ± 3.0	0.9
$3/2 \rightarrow 1/2_1$	393.4 ± 2.0	-0.4	$5/2_2 \rightarrow 7/2_1$	478.2 ± 2.0	-1.1
Transition $R_3(2)$			$7/2_2 \rightarrow 7/2_1$	528.3 ± 2.5	-0.8
$3/2_1 \rightarrow 5/2_2$	87.2 ± 2.0	-0.1	$3/2 \rightarrow 5/2$	579.4 ± 2.0	0.4
$5/2 \rightarrow 5/2_2$	144.6 ± 2.5	0.8	$5/2_2 \rightarrow 5/2$	618.1 ± 2.5	0.1
$1/2_1 \rightarrow 3/2_2$ }			Transition $R_3(5)$		
$3/2_1 \rightarrow 5/2_1$ }	191.8		$9/2_1 \rightarrow 11/2_2$	127.1 ± 2.0	-0.3
$3/2_2 \rightarrow 5/2_2$	234.9 ± 5.0	2.7	$9/2_1 \rightarrow 11/2_1$	211.4 ± 3.0	0.3
$5/2 \rightarrow 5/2_1$	254.2 ± 3.0	2.4	$7/2_1 \rightarrow 9/2_2$	244.8 ± 2.0	1.1
$1/2_2 \rightarrow 3/2_2$	300.8 ± 2.5	-0.3	$9/2_2 \rightarrow 11/2_1$	352.7 ± 2.0	-0.4
$3/2_2 \rightarrow 5/2_1$	342.2 ± 2.5	2.0	$7/2_2 \rightarrow 9/2_1$	485.8 ± 2.0	-0.9
$1/2_2 \rightarrow 3/2_1$	440.7 ± 5.0	-0.1	$9/2_2 \rightarrow 9/2_1$	532.0 ± 3.5	-2.2
$3/2_2 \rightarrow 3/2_1$	507.8 ± 2.5	1.6	$5/2 \rightarrow 7/2$	595.5 ± 2.0	1.1
$1/2_2 \rightarrow 1/2$	539.4 ± 2.5	0.2	$7/2_2 \rightarrow 7/2$	634.0 ± 3.0	-0.8
$3/2_2 \rightarrow 1/2$	605.4 ± 3.0	0.8	Transition $R_3(6)$		
Transition $R_3(3)$			$11/2_1 \rightarrow 13/2_2$	130.3 ± 2.0	-1.2
$5/2_1 \rightarrow 7/2_2$	108.2 ± 2.0	-1.2	$13/2 \rightarrow 13/2_2$	176.0 ± 6.0	-1.1
$7/2 \rightarrow 7/2_2$	159.0 ± 2.5	-1.8	$11/2_1 \rightarrow 13/2_1$	216.0 ± 2.5	1.5
$3/2_1 \rightarrow 5/2_2$	215.3 ± 5.0	-1.1	$9/2_1 \rightarrow 11/2_2$	252.6 ± 2.0	1.5
$7/2 \rightarrow 7/2_1$]			$11/2_2 \rightarrow 13/2_2$	271.4 ± 5.0	-1.2
$5/2_1 \rightarrow 5/2_2$ }	252.4		$11/2_1 \rightarrow 11/2_2$	292.7 ± 4.0	-0.1
$5/2_2 \rightarrow 7/2_2$]			$11/2_2 \rightarrow 13/2_1$	355.0 ± 2.0	-0.6
$5/2_2 \rightarrow 7/2_1$	345.6 ± 2.0	-0.9	$9/2_2 \rightarrow 11/2_2$	390.2 ± 3.5	2.4
$5/2_1 \rightarrow 5/2_1$	375.6 ± 2.5	-1.2	$9/2_2 \rightarrow 11/2_1$	491.2 ± 2.0	-0.6
$3/2_2 \rightarrow 5/2_1$	466.6 + 2.0	-0.6	$11/2_2 \rightarrow 11/2_1$	536.1 + 3.0	-1.9
$5/2_2 \rightarrow 5/2_1$	520.8 + 3.0	-0.6	$7/2 \rightarrow 9/2$	606.0 ± 2.0	0.8
$1/2 \rightarrow 3/2$	554.5 + 3.5	-0.9	$9/2_2 \rightarrow 9/2$	645.4 ± 3.5	1.1
$3/2_2 \rightarrow 3/2$	590.3 + 3.5	-0.9	Transition $R_3(7)$		
Transition $R_3(4)$			$13/2_1 \rightarrow 15/2_2$	135.1 ± 2.0	-2.5
$7/2_1 \rightarrow 9/2_2$	121.0 ± 2.0	0.1	$11/2_1 \rightarrow 13/2_2$	259.2 ± 2.0	2.7
$9/2 \rightarrow 9/2_2$	170.3 ± 2.5	0.9	$13/2_2 \rightarrow 15/2_1$	360.0 ± 2.0	2.2

APPENDIX B. (*Concluded*)

F" → F'	Obs. Freq.	Obs-Calc.
$11/2_2 \rightarrow 13/2_1$	497.7 ± 2.0	2.0
$9/2 \rightarrow 11/2$	615.0 ± 3.0	3.0
Transition $^{Q}P_{32}(3)$		
$7/2_1 \rightarrow 5/2_2$	56.1 ± 3.5	-2.5
$5/2_1 \rightarrow 3/2_2$	94.1 ± 2.5	0.1
$7/2_2 \rightarrow 5/2_1$	182.7 ± 2.5	-2.3
$5/2_2 \rightarrow 3/2_1$	245.8 ± 2.5	-2.9
$3/2 \rightarrow 1/2$	275.2 ± 3.0	-1.1
Transition $^{Q}P_{32}(4)$		
$9/2_1 \rightarrow 7/2_2$	75.1 ± 2.5	0.3
$7/2_1 \rightarrow 5/2_2$	123.0 ± 2.0	-0.4
$9/2_2 \rightarrow 7/2_1$	200.3 ± 2.5	0.2
$7/2_2 \rightarrow 5/2_1$	278.2 ± 2.5	-0.3
$5/2 \rightarrow 3/2$	322.8 ± 3.0	0.9
Transition $^{Q}P_{32}(5)$		
$11/2_1 \rightarrow 9/2_2$	85.1 ± 2.0	-0.2
$9/2_1 \rightarrow 7/2_2$	142.6 ± 2.5	-0.8
$11/2_2 \rightarrow 9/2_1$	208.6 ± 2.0	-1.3
$9/2_2 \rightarrow 7/2_1$	297.2 ± 2.5	-0.5
$7/2 \rightarrow 5/2$	352.4 ± 2.5	0.2
Transition $^{Q}P_{32}(6)$		
$13/2_1 \rightarrow 11/2_2$	92.3 ± 2.0	-0.1
$11/2_1 \rightarrow 9/2_2$	156.9 ± 2.5	-0.9
$13/2_2 \rightarrow 11/2_1$	216.1 ± 2.0	-0.7
$11/2_2 \rightarrow 9/2_1$	312.3 ± 2.0	1.2
$9/2 \rightarrow 7/2$	374.5 ± 2.0	0.7
Transition $P_3(3)$		
$5/2_1 \rightarrow 5/2$	-51.5 ± 2.5	-0.2
$5/2_1 \rightarrow 3/2_2$	54.1 ± 2.0	0.4
$5/2_2 \rightarrow 5/2$	94.1 ± 2.5	0.9
$3/2_1 \rightarrow 1/2_2$	129.1 ± 2.5	-0.5
$3/2_1 \rightarrow 3/2_1$	161.9 ± 3.0	-0.7
$5/2_1 \rightarrow 3/2_1$, $5/2_2 \rightarrow 3/2_2$	199.5	
$1/2 \rightarrow 3/2_1$, $3/2_2 \rightarrow 1/2_2$	256.1	
$3/2_2 \rightarrow 3/2_1$	289.4 ± 3.5	-0.3
$3/2_1 \rightarrow 1/2_1$	305.7 ± 5.0	1.4
$5/2_2 \rightarrow 3/2_1$	344.9 ± 2.0	1.0
$1/2 \rightarrow 1/2_1$	397.9 ± 2.5	0.8
$3/2_2 \rightarrow 1/2_1$	432.8 ± 3.0	-0.1

"Observed hyperfine splittings (in megahertz) for NH in $A^3\Pi$, $v = 0 \leftarrow X^3\Sigma^-$, $v = 0$ transitions, and deviations from the values obtained in a least squares fit. The splittings are all given in series of one rotational transition and they are relative to the $F'' = J'' - 3/2 \rightarrow F' = J' + 3/2$ line. The quantum numbers F'' and F' refer to the ground and excited states respectively, while (1) and (2) refer to states with the same quantum number for upper and lower energy. The lines without a value in the last column were not taken into the data set of the computer program because of severe overlap. For the $R_1(2)$ transition, only those components that are not overlapped by the $^{R}Q_{21}(1)$ transition are given.